# Angle-Resolved Nanosphere Lithography: Manipulation of Nanoparticle Size, Shape, and Interparticle Spacing

**Christy L. Haynes,[†] Adam D. McFarland,[†] Matthew T. Smith,[‡] John C. Hulteen,[§] and Richard P. Van Duyne***

*Department of Chemistry, Northwestern University, Evanston, Illinois 60208-3113*

*Received: September 19, 2001; In Final Form: December 3, 2001*

This work presents a novel approach to fine-tuning the size, shape, and interparticle spacing of nanoparticles fabricated by nanosphere lithography (NSL). This approach, termed angle-resolved nanosphere lithography (AR NSL), is a variant of NSL that yields vastly different, and increasingly flexible, nanostructures. This is accomplished by controlling the angle, $\theta$, between the surface normal of the sample assembly and the propagation vector of the material deposition beam. Comparison of experimental results to simulated nanoparticle array geometries generated using an analytical model show excellent qualitative agreement. Using AR NSL, we have demonstrated that it is possible to reduce in-plane nanoparticle dimensions by a factor of 4. This important result shows that it will be possible to achieve fabrication of nanoparticles with precision control of their dimensions in a size regime comparable with the industry standard electron beam lithography. AR NSL provides a massively parallel, rather than serial, nanoparticle fabrication method. One limitation of the AR NSL technique is the inability to pattern an entire substrate with a single nanoparticle geometry without control of the mask domain orientation. While the presence of multiple domains in any given colloidal crystal mask complicates the fabrication of large-area homogeneous nanoparticle arrays, this quality is, in fact, useful in laboratory scale experiments requiring a diverse set of nanostructure features on a single sample. The precision tuning of nanoparticle size, shape, and spacing that can be achieved in a massively parallel, materials/substrate general, and inexpensive fashion using AR NSL is likely to have significant impact on the fields of surface-enhanced spectroscopy, near field optical microscopy, nanoscopic object manipulation, and chemical/biological sensing.

## I. Introduction

Nanotechnology research is driven by the demand for ever smaller device features needed to achieve improved performance and decreased cost in the microelectronics, communications, and data storage industries. Developments in nanotechnology rely on the design and fabrication of nanostructures with features in the 1−100 nm size regime. The ideal nanofabrication technique would be materials and substrate general, inexpensive, flexible in nanoparticle size, shape, and spacing parameters, and massively parallel. Several standard lithographic methods are routinely used to create nanostructures with controlled size, shape, and interparticle spacing with varying success.[1−8]

Nanosphere lithography (NSL) is the second generation innovation of the technique originally known as "natural lithography",[9,10] where a monodisperse nanosphere template acts as a deposition mask.[11] NSL is an inexpensive, inherently parallel, high-throughput, and materials general nanofabrication technique that is now being employed in laboratories around the world.[12,13] The homogeneous arrays of nanoparticles produced using NSL are potentially useful in studies of size-dependent optical,[14−17] magnetic,[18,19] catalytic,[20−23] thermodynamic,[24,25] electrochemical,[26] and electrical transport[27−29] properties of materials. The perceived limitations of NSL are (1) that it is capable of producing only a limited range of nanoparticle shapes and interparticle spacing and (2) that there is an inherent size limitation due to the increasing polydispersity involved in the synthesis of smaller diameter nanospheres (viz. 10−100 nm range) necessary to grow the 2D colloidal crystal.

The conventional NSL process begins with self-assembly of a nanosphere mask onto a substrate followed by line-of-sight deposition of a material(s) through the mask. In general, the substrate to be patterned is positioned normal to the direction of material deposition. The resultant nanoparticles have an in-plane shape and interparticle spacing determined by the projection of the nanosphere mask interstices onto the substrate. A monolayer mask produces nanoparticles having a triangular in-plane shape arranged on the surface with *p*6*mm* symmetry. The ratio of the interparticle spacing to the in-plane perpendicular bisector is a fixed value, ca. 2.5.

Angle-resolved nanosphere lithography (AR NSL) is a simple variant on conventional NSL producing vastly different, and increasingly flexible, nanostructures by control of the angle between the surface normal of the sample assembly and the propagation vector of the material deposition beam ($\theta$). Figure 1 demonstrates how the size, shape, and spacing of the projected nanosphere interstices vary at three representative $\theta$ values. Regulating the angle between a substrate and the direction of material deposition has previously been used to produce other nanofabricated surfaces, such as field effect transistors,[30,31] single electron transistors,[32] ultrasmall tunnel junctions,[33,34] ultrahigh-resolution magnetic force microscopy probes,[35] DNA-based

* To whom correspondence should be addressed. E-mail: vanduyne@chem.northwestern.edu.
[†] These authors contributed equally to this work.
[‡] Union Carbide, South Charleston, WV.
[§] 3M Corporation, St. Paul, MN.

10.1021/jp013570+ CCC: $22.00 
Published on Web 01/31/2002

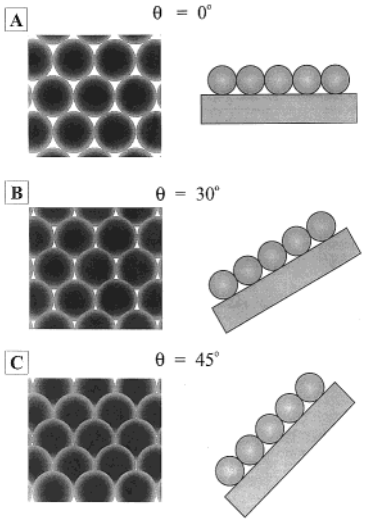


**Figure 1.** Schematic illustration showing top and side views of nanosphere masks used for AR NSL at $\theta = 0°$, 30°, and 45° and $\phi = 0°$.

electrical circuits,[36] and optical coatings.[37] Robbie et al.[38] have developed a similar technique known as glancing angle deposition (GLAD) to fabricate thin films with controlled porosity. Similarly, Skaife and co-workers have controlled ultrathin gold film topography using oblique deposition.[39]

This paper demonstrates that AR NSL can be used to manipulate the size, shape, and spacing of nanoparticles while maintaining the aforementioned strengths of conventional NSL. Furthermore, a geometric model of AR NSL is developed here and used to demonstrate that the projection of the mask interstices change in a systematic fashion based on deposition angle, $\theta$, and azimuthal angle of the mask, $\phi$.

The remainder of this paper is organized as follows. In section II, the AR NSL and characterization techniques are described explicitly. In section III, an analytic AR NSL geometric model is presented. Section IV demonstrates representative examples of the variety of nanoparticle sizes, shapes, and spacings made feasible with AR NSL. Although many materials could have been used to illustrate the structural characterization of AR NSL-fabricated nanoparticles, Ag and Cr nanoparticles are presented throughout section IV as the model systems. The good agreement between the structural characteristics of fabricated nanoparticles probed by FE-SEM and AFM and the model presented in section III is also demonstrated. In section V, our results and conclusions are summarized. The analytical model, Maple 6 code, is included as Supporting Information.

## II. Experimental Section

**A. Materials.** N-doped Si(111) (4.25−8.5 $\Omega$ cm$^{-1}$ ) was purchased from Silicon Quest International (Santa Clara, CA) and cut into ~2 cm$^2$ pieces. Borosilicate glass substrates were No. 2 coverslips purchased from Fisher Scientific (Fairlawn, VA). Pretreatment of substrates required $H_2SO_4$, $H_2O_2$, and $NH_4OH$, all purchased from Fisher Scientific (Fairlawn, VA). For all steps of substrate preparation, ultrapure water (18.2 M$\Omega$ cm$^{-1}$) from a Millipore Academic system (Marlborough, MA) was used. Nanospheres were surfactant-free white carboxyl polystyrene latex solutions acquired from Interfacial Dynamics Corporation (Portland, OR) and were used as received (10% solid suspension). Chrome plated tungsten rods and tungsten deposition boats were purchased from R. D. Mathis (Long Beach, CA). Ag (99.9%) was purchased from D. F. Goldsmith (Evanston, IL). Sonication to remove nanosphere masks was done in absolute ethanol purchased from Pharmco (Brookfield, CT).

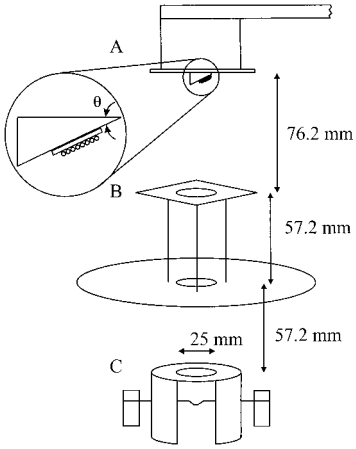


**Figure 2.** Schematic diagram of the apparatus used for AR NSL: (A) quartz crystal microbalance and sample assembly, (B) collimation plates, and (C) the thermal atomic source.

**B. Self-Assembly of 2D Colloidal Crystal Masks.** Both the Si(111) and borosilicate glass substrates were pretreated in two steps: (1) pirahna etch, 3:1 $H_2SO_4$:30% $H_2O_2$ at 80° C for 1 h, was used to clean the substrate, and (2) base treatment, 5:1:1 $H_2O$:$NH_4OH$:30% $H_2O_2$ with sonication for 1 h, was used to render the surface hydrophilic. Approximately 4.5 $\mu$L (silicon substrates) or 2.5 $\mu$L (glass substrates) of undiluted nanosphere solution, nanosphere diameter of 951 ± 33 nm, were drop coated onto each substrate and allowed to dry in ambient conditions.

**C. Physical Vapor Deposition of Cr and Ag Overlayers.** The metal films were deposited in a modified Consolidated Vacuum Corp. vapor deposition system[40] (Figure 2) with a base pressure of $10^{-7}$ Torr. The mass thickness and deposition rate for each film were measured using a Leybold Inficon XTM/2 quartz-crystal microbalance (QCM) (East Syracuse, NY). Samples were mounted 240 mm above the effusive source with three 25 mm diameter apertures regularly spaced between the source and the sample to provide collimation of the physical vapor deposition beam. $\theta$, the angle between the surface normal of the sample assembly and the propagation vector of the material deposition beam, was controlled by mounting the samples on machined Al blocks (Figure 2). After metal deposition, removal of the polystyrene nanospheres was achieved by sonication in absolute ethanol for 3 min.

**D. FE-SEM and AFM Measurements.** All field emission scanning electron microscope (FE-SEM) images were acquired using a Hitachi S4500-II equipped with a cold-field emission gun and a through-the-lens secondary electron detector. For all measurements, the accelerating voltage was 5 kV and the emission current was 10 $\mu$A. All images were captured and processed using the IMIX Microanalysis Imaging System (Princeton Gamma-Tech, Princeton, NJ).

All atomic force microscopy (AFM) images were collected in ambient conditions with a Digital Instruments Nanoscope III AFM. The etched Si nanoprobe tips (Digital Instruments, Santa Barbara, CA) used to acquire the images have resonant frequencies between 285 and 315 kHz. These tips are conical in shape with a cone angle of 20° and a effective radius of curvature of 10 nm. The sharp features of these tips were necessary to reduce tip-induced image broadening and to decrease the effect of capillary forces with the surface. The images reported herein are raw, unfiltered data collected in the

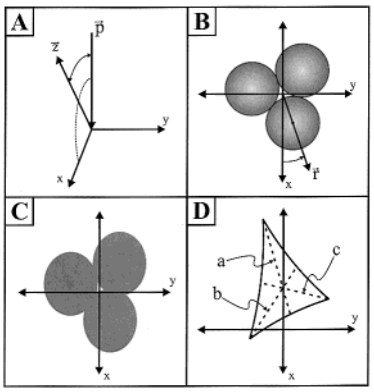


**Figure 3.** Coordinate system and parameters for the geometric modeling of AR NSL. (A) The coordinate system used to define $\theta$. The substrate lies in the *xy* plane, $\vec{z}$ is the vector normal to the substrate, and $\vec{p}$ is the propagation vector of the material deposition beam. $\theta$, referred to in the text as the inclination angle, is the acute angle between $\vec{p}$ and $\vec{z}$. (B) Illustration of close-packed nanospheres with centers located equidistant from the origin of the coordinate system. $\phi$, the azimuthal angle, is defined as the acute angle between the *x* axis and $\vec{r}$, the vector from the origin to the center of the nanosphere nearest the *x* axis. (C) The projection of the nanosphere mask onto the *xy* plane (substrate) along $\vec{p}$ ($\theta = 30°$). (D) Illustration of the projected interstice designating angle bisectors *a*, *b*, and *c*.

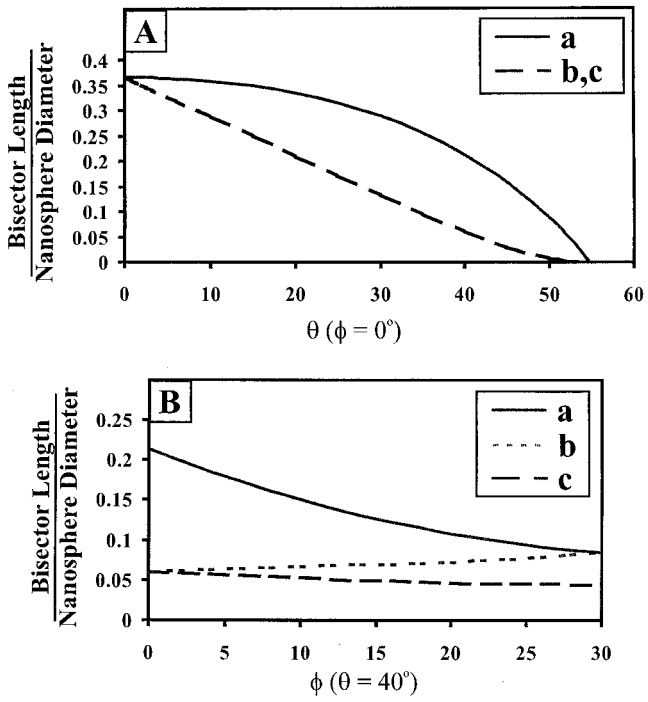


**Figure 4.** Calculated dependence of angle bisector lengths (*a*, *b*, and *c*) on (A) $\theta$ with fixed $\phi = 0°$ and (B) $\phi$ with fixed $\theta = 40°$.

intermittent contact mode using a scan rate of 2.44 Hz. The scan head had a range of 13 $\mu$m × 13 $\mu$m.

### III. Modeling of AR NSL-Fabricated Nanoparticle Shapes and Dimensions

The symbolic mathematics program Maple 6 (Version 6.01, Waterloo Maple Inc., Ontario, Canada) was used to model nanoparticle shapes generated with AR NSL. The worksheet that was used to accomplish this consisted of the following routines: (1) determining the projection of a nanosphere mask onto a substrate for specified $\theta$ and $\phi$ (Figure 3), (2) solving for the intersection of the nanosphere projections which corresponds to the tips of the fabricated nanoparticles, and (3) using simple plane geometry to calculate the lengths of the nanoparticles' angle bisectors. The program was also used to generate graphical representations of the nanoparticle shapes in order to qualitatively compare our model with nanoparticle shapes observed with FE-SEM. In all cases, the azimuthal angle $\phi$, defining the nanosphere mask registry on the substrate, was chosen to give best qualitative agreement with overall shape for the experimentally controlled $\theta$ value.

### IV. Results and Discussion

Using the model described in section III, the expected behavior of nanoparticle angle bisector lengths (*a*, *b*, *c*) was generated for many different deposition geometries. Figure 4A shows calculated bisector lengths as a function of mask inclination ($\theta$) while holding mask registry constant, $\phi = 0°$. In this case, the projected interstices close to line-of-sight deposition at $\theta = 54.74°$. While $\theta$ is easily controlled by deposition geometry, imperfections in nanosphere mask crystallization present difficulty in controlling mask registry (denoted by $\phi$ values). Variations in mask registry greatly affect the fabricated nanoparticle geometry, as demonstrated in Figure 4B. Because of the inability to control nanosphere mask domain registry, a wide variety of nanoparticle shapes and sizes are produced by AR NSL on each substrate. If it were possible to control the template registry, deposition through a 140 nm diameter nanosphere mask, currently the smallest we have used,[41] at $\theta = 40°$ would produce nanoparticles with an average bisector length of 10 nm.

Figure 5 depicts four examples of AR NSL-generated nanoparticle arrays. The simulated nanoparticle shape is overlaid on the actual nanoparticle positions in the panels on the right. Note that when the nanosphere mask registry approaches $\phi = 0°$, as in Figure 5B,D, one bisector length becomes significantly longer than the other two. As $\phi$ approaches 30°, as shown in Figure 5A, two bisector lengths are significantly longer than the third. At intermediate $\phi$ angles, as represented in Figure 5C, all nanoparticle dimensions are distinctly unique. It is apparent in the presented FE-SEM images that nanoparticle features exhibit a finite radius of curvature. This tip rounding results in nanoparticle dimensions that are smaller than those predicted with the geometric model.

While the interparticle spacing is constant for samples with $\theta = 0°$, there is great variation in nanoparticle spacing for AR NSL-fabricated arrays. Table 1 shows measured interparticle spacings for each of the arrays shown in Figure 5. Deposition angle, mask registry, and tip rounding drastically affect the measured interparticle spacing.

To validate the AR NSL approach to nanoparticle fabrication in the regime usually addressed by electron beam lithography, high-angle depositions were performed in order to yield nanoparticles greatly reduced in size in comparison to a $\theta = 0°$ condition. Atomic force microscopy (AFM) was implemented in order to get precise measurement of nanoparticles fabricated at large $\theta$ values. Figure 6 displays a topographic image of an AR NSL array ($\theta = 40°$, $\phi = 0°$) and two height profile line scans. Accounting for AFM tip convolution of 20 nm,[41] the average length of the nanoparticles' longest bisector is approximately 100 nm. This is a reduction by a factor of 2.5 in size from the $\theta = 0°$ condition. The average length of the nanoparticles' two short bisectors is approximately 65 nm, a factor of 4 size reduction from the $\theta = 0°$ condition. Figure 6

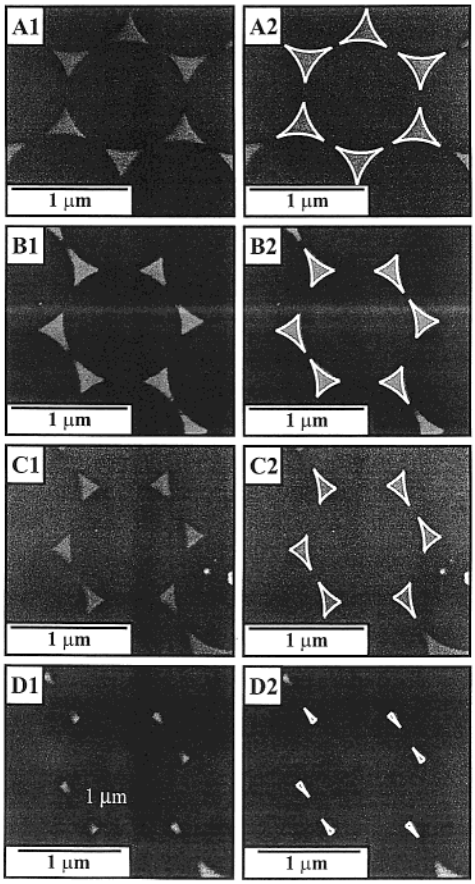


**Figure 5.** Field emission scanning electron micrographs of AR NSL-fabricated nanoparticle arrays and images with simulated geometry superimposed, respectively. (A1, A2) $\theta = 10°$, $\phi = 28°$, (B1, B2) $\theta = 20°$, $\phi = 2°$, (C1, C2) $\theta = 26°$, $\phi = 16°$, and (D1, D2) $\theta = 40°$, $\phi = 2°$. All samples are Cr deposited onto Si(111) substrates. Images were collected at 40k magnification.

**TABLE 1: Interparticle Spacings for Nanoparticle Arrays Shown in Figure 5**

| | short interparticle spacing | long interparticle spacing |
|---|---|---|
| $\theta$ (deg) | nanosphere diameter | nanosphere diameter |
| 10 | 0.155 | 0.218 |
| 20 | 0.064 | 0.290 |
| 26 | 0.183 | 0.391 |
| 40 | 0.264 | 0.603 |

represents the most drastic size reduction and variation of interparticle spacing witnessed to date using AR NSL. Although these nanoparticle sizes are not representative of the electron beam lithography size regime, application of similar experimental conditions to smaller nanosphere diameter masks (i.e., nanosphere diameter of 325 nm) would reach nanoparticle dimensions less than 20 nm.

To evaluate the overall efficacy of our model's ability to quantitatively predict nanoparticle dimensions, measured nanoparticle dimensions were compared to theoretical dimension boundaries. Boundary conditions were implemented due to the uncertainty in assigning a $\phi$ value to an imaged nanoparticle domain. The largest and smallest possible bisector lengths were plotted as a function of $\theta$ while holding $\phi$ equal to 0° and 30°, respectively. Figure 7 shows the theoretical bisector length bounds as well as all measured bisector lengths. The measured data points are clustered closer to the lower boundary (with one measured bisector falling below the theoretical limit). This behavior can be attributed to the aforementioned tip rounding

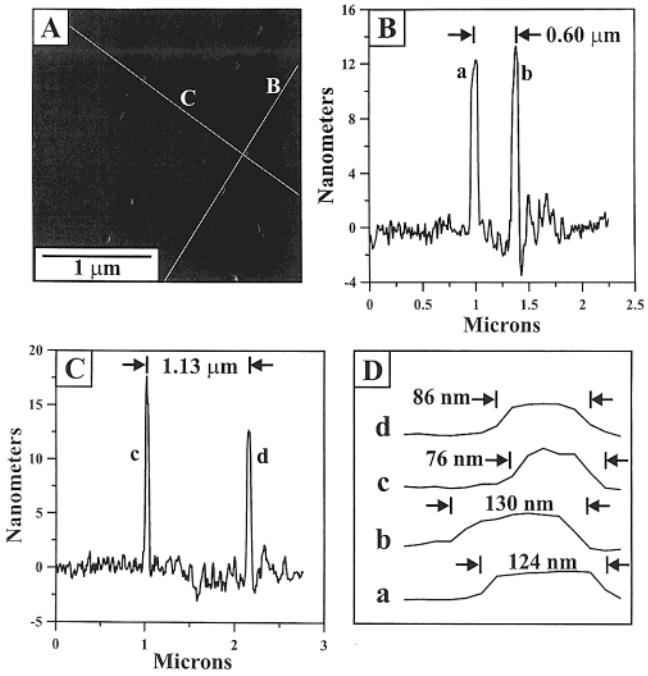


**Figure 6.** (A) Atomic force microscope image (2.44 $\mu$m × 2.44 $\mu$m), (B, C) line scans indicated in (A), and (D) line scan expansions indicated in (B, C) of Ag nanoparticles on borosilicate glass fabricated with 951 nm diameter nanosphere mask ($\theta = 40°$, and $\phi = 0°$).

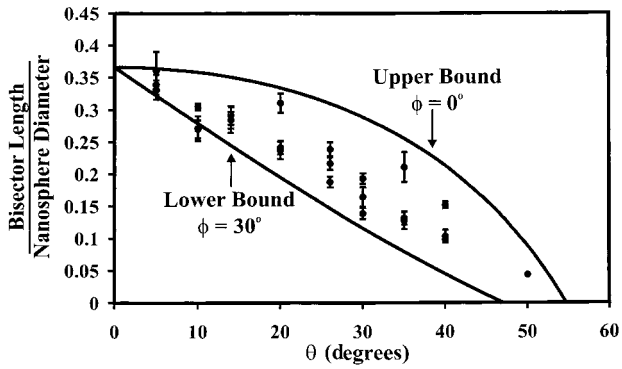


**Figure 7.** Calculated dependence of angle bisector length bounds with experimentally measured bisector lengths superimposed. The upper boundary is the longest bisector length with $\phi = 0°$. The lower boundary is the shortest bisector length with $\phi = 30°$.

effect. Note that the lower bound actually goes to zero at approximately $\theta = 47°$. This lower boundary condition, in addition to the inability to control mask registry, made it difficult to locate nanoparticles fabricated with large $\theta$ values.

## V. Conclusions

Herein we present angle-resolved nanosphere lithography (AR NSL), a novel technique in lithographic nanoscale surface design that expands the size and shape tunability of conventional nanosphere lithography (NSL) as well as allowing for, before impossible, variation of interparticle spacing. Experimental results were compared to simulated nanoparticle array geometries generated using an analytical model. Qualitatively, the model performed well at reproducing nanoparticle array geometry; however, the inability to control nanosphere mask registry, the azimuthal angle $\phi$, presented difficulties in using the model to quantitatively predict nanoparticle sizes. It is evident from measured data that the invariable nanoparticle spacing of

conventional NSL is easily manipulated using AR NSL, thus allowing for future experiments which require variable electromagnetic coupling between nanoparticles.

Another advantage of AR NSL over the conventional NSL technique is its ability to yield nanoparticles within the size regime conventionally fabricated by electron beam lithography. While conventional NSL 2D colloidal crystal mask formation is limited by the inherent polydispersity of small diameter nanospheres (viz., 10−100 nm), AR NSL has been demonstrated to reduce nanoparticle dimensions by up to a factor of 4, allowing for fabrication of electron beam lithography size regime nanoparticles with easily prepared nanosphere masks. Because all of the experimentally measured nanoparticle dimensions show good agreement with the theoretical bounds, variation of sample inclination ($\theta$) can be used as a coarse adjustment of nanoparticle geometry and spacing.

The major obstacle encountered when using AR NSL is the inability to control mask registry, $\phi$. Because 2D colloidal crystal growth results in multiple hexagonally close-packed domains with random orientations, nanoparticle shape, size, and spacing vary over any given sample. More elaborate nanosphere mask preparation techniques, such as template-assisted assembly,[42] will allow fabrication of nanoparticle arrays with specific geometries; this work is the subject of future publication. While the presence of multiple domains complicates the fabrication of large-area homogeneous nanoparticle arrays, it is useful in experiments requiring a diverse set of nanostructure features on a single sample. For instance, the multiple domains created on a single AR NSL-fabricated surface can be sampled in order to locate areas with specifically desired characteristics (e.g., magnetic, optical, topographic characteristics).

In conclusion, AR NSL vastly expands the conventional NSL nanofabrication technique. This simple, inexpensive, massively parallel and material/substrate-general tool offers an alternative procedure to fabricate nanoparticles approaching the electron beam lithography size regime.

**Acknowledgment.** We acknowledge the support of the National Science Foundation (CHE-940078), the MRSEC program of the National Science Foundation (DMR-9632472 and DMR-0076097) at the Materials Research Center of Northwestern University, and the Army Research Office MURI program (DAAG-55-97-0133). C.L.H. gratefully acknowledges the support of GlaxoSmithKline and the ACS Division of Analytical Chemistry.

**Supporting Information Available:** The analytical model, Maple 6 code. This material is available free of charge via the Internet at http://pubs.acs.org.

## References and Notes

(1) Wallraff, G. M.; Hinsberg, W. D. *Chem. Rev.* **1999**, *99*, 1801−1821.

(2) Ito, T.; Okazaki, S. *Nature* **2000**, *406*, 1027−1031.

(3) Bloomstein, T. M.; Horn, M. W.; Rothschild, M.; Kunz, R. R.; Palmacci, S. T.; Goodman, R. B. *J. Vac. Sci. Technol. B* **1997**, *15*, 2112−2116.

(4) Liao, P. F.; Bergman, J. G.; Chemla, D. S.; Wokaun, A.; Melngailis, J.; Hawryluk, A. M.; Economou, N. P. *Chem. Phys. Lett.* **1981**, *81*, 355−359.

(5) Liao, P. F. Silver Structures Produced by Microlithography. In *Surface Enhanced Raman Scattering*; Chang, R. K., Furtak, T. E., Eds.; Plenum Press: New York, 1982; pp 379−390.

(6) Howard, R. E.; Liao, P. F.; Skocpol, W. J.; Jackel, L. D.; Craighead, H. G. *Science* **1983**, *221*, 117−121.

(7) Kitson, S. C.; Barnes, W. L.; Sambles, J. R. *IEEE Photonics Technol. Lett.* **1996**, *8*, 1662−1664.

(8) Smith, H. I.; Schattenburg, M. L. *IBM J. Res. Dev.* **1993**, *37*, 319−329.

(9) Fischer, U. C.; Zingsheim, H. P. *J. Vac. Sci. Technol.* **1981**, *19*, 881−885.

(10) Deckman, H. W.; Dunsmuir, J. H. *Appl. Phys. Lett.* **1982**, *41*, 377−379.

(11) Hulteen, J. C.; Van Duyne, R. P. *J. Vac. Sci. Technol. A* **1995**, *13*, 1553−1558.

(12) Frey, W.; Woods, C. K.; Chilkoti, A. *Adv. Mater.* **2000**, *12*, 1515−1519.

(13) Wiesendanger, R.; Bode, M.; Kleiber, M.; Lahndorf, M.; Pascal, R.; Wadas, A. *J. Vac. Sci. Technol. B* **1997**, *15*, 1330−1334.

(14) Mulvaney, P. *Langmuir* **1996**, *12*, 788−800.

(15) Grabar, K. C.; Smith, P. C.; Musick, M. D.; Davis, J. A.; Walter, D. G.; Jackson, M. A.; Guthrie, A. P.; Natan, M. J. *J. Am. Chem. Soc.* **1996**, *118*, 1148−1153.

(16) Feldstein, M. J.; Keating, C. D.; Liau, Y.-H.; Natan, M. J.; Scherer, N. F. *J. Am. Chem. Soc.* **1997**, *119*, 6638−6647.

(17) Kreibig, U. Optics of Nanosized Metals. In *Handbook of Optical Properties. Optics of Small Particles, Interfaces, and Surfaces*; Hummel, R. E., Wissmann, P., Eds.; CRC Press: Boca Raton, FL, 1997; Vol. II, pp 145−190.

(18) New, R. M. H.; Pease, R. F. W.; White, R. L. *J. Vac. Sci. Technol. B* **1995**, *13*, 1089−1094.

(19) Shi, J.; Gider, S.; Babcock, K.; Awschalom, D. D. *Science* **1996**, *271*, 937−941.

(20) Bradley, J. S. The Chemistry of Transition Metal Colloids. In *Clusters and Colloids From Theory to Applications*; Schmid, G., Ed.; VCH Publishers: New York and Weinheim, 1994; pp 459−544.

(21) Street, S. C.; Xu, C.; Goodman, D. W. *Annu. Rev. Phys. Chem.* **1997**, *48*, 43−68.

(22) Heiz, U.; Vanolli, F.; Sanchez, A.; Schneider, W. D. *J. Am. Chem. Soc.* **1998**, *120*, 9668−9671.

(23) Yang, M. X.; Gracias, D. H.; Jacobs, P. W.; Somorjai, G. A. *Langmuir* **1998**, *14*, 1458−1464.

(24) Volokitin, Y.; Sinzig, J.; de Jongh, L. J.; Schmid, G.; Vargaftik, M. N.; Moiseev, I. I. *Nature* **1996**, *384*, 621−623.

(25) Wang, Z. L.; Petroski, J. M.; Green, T. C.; El-Sayed, M. A. *J. Phys. Chem. B* **1998**, *102*, 6145−6151.

(26) Gorer, S.; Ganske, J. A.; Hemminger, J. C.; Penner, R. M. *J. Am. Chem. Soc.* **1998**, *130*, 9584−9593.

(27) Alivisatos, A. P. *J. Phys. Chem.* **1996**, *100*, 13226−13239.

(28) Bezryadin, A.; Dekker, C.; Schmid, G. *Appl. Phys. Lett.* **1997**, *71*, 1273−1275.

(29) Andres, R. P.; Bielefeld, J. D.; Henderson, J. I.; Janes, D. B.; Kolagunta, V. R.; Kubiak, C. P.; Mahoney, W. J.; Osifchin, R. G. *Science* **1996**, *273*, 1690−1693.

(30) Dickmann, J.; Geyer, A.; Daembkes, H.; Nickel, H.; Loesch, R.; Schlapp, W. *J. Electrochem. Soc.* **1991**, *138*, 491−493.

(31) Strifler, W. A.; Cantos, B. D. *J. Vac. Sci. Technol. B* **1990**, *8*, 1297−1299.

(32) Kenyon, M.; Amar, A.; Song, D.; Lobb, C. J.; Wellstood, F. C. *Appl. Phys. Lett.* **1998**, *72*, 2268−2270.

(33) Wada, T.; Haraichi, S.; Ishii, K.; Hiroshima, H.; Komuro, M.; Hirayama, M. *J. Vac. Sci. Technol. A* **1996**, *14*, 1850−1854.

(34) Wada, T.; Haraichi, S.; Ishii, K.; Hiroshima, H.; Komuro, M.; Gorwadkar, S. M. *J. Vac. Sci. Technol. A* **1998**, *16*, 1430−1434.

(35) Fischer, P. B.; Wei, M. S.; Chou, S. Y. *J. Vac. Sci. Technol. B* **1993**, *11*, 2570−2573.

(36) Di Mauro, E.; Hollenberg, C. P. *Adv. Mater.* **1993**, *5*, 384−386.

(37) Mbise, G. W.; Le Bellac, D.; Niklasson, G. A.; Granqvist, C. G. *J. Phys. D: Appl. Phys.* **1997**, *30*, 2103−2122.

(38) Robbie, K.; Sit, J. C.; Brett, M. J. *J. Vac. Sci. Technol. B* **1998**, *16*, 1115−1122.

(39) Skaife, J. J.; Brake, J. M.; Abbott, N. L. *Langmuir* **2001**, *17*, 5448−5457.

(40) Hulteen, J. C. I. Surface-Enhanced Hyper-Raman Spectroscopy. II. Nanosphere Lithography. Ph.D. Thesis, Northwestern University, 1995.

(41) Hulteen, J. C.; Treichel, D. A.; Smith, M. T.; Duval, M. L.; Jensen, T. R.; Van Duyne, R. P. *J. Phys. Chem. B* **1999**, *103*, 3854−3863.

(42) Yin, Y.; Lu, Y.; Gates, B.; Xia, Y. *J. Am. Chem. Soc.* **2001**, *123*, 8718−8729.